The Astrophysical Journal, 908:63 (7pp), 2021 February 10 https://doi.org/10.3847/1538-4357/abd315

Search for Radio Remnants of Nearby Off-axis Gamma-Ray Bursts in a Sample of Swift/BAT Events

C. Grandorf[1], J. McCarty[1], P. Rajkumar[1], H. Harbin[1], K. H. Lee[2], A. Corsi[1], I. Bartos[2], Z. Márka[3], A. Balasubramanian[1], and S. Márka[4]

[1] Department of Physics and Astronomy, Texas Tech University, Box 1051, Lubbock, TX 79409-1051, USA; Connor.Grandorf@ttu.edu,ConnorGrandorf@my.unt.edu, jmccarty@mit.edu
[2] Department of Physics, University of Florida, Gainesville, FL 32611-8440, USA; kyunghwanlee@ufl.edu
[3] Columbia Astrophysics Laboratory, Columbia University in the City of New York, New York, NY 10027, USA
[4] Department of Physics, Columbia University in the City of New York, New York, NY 10027, USA
Received 2020 August 13; revised 2020 December 8; accepted 2020 December 11; published 2021 February 15

Abstract

The multi-messenger discovery of gravitational waves (GWs) and light from the binary neutron star (NS) merger GW170817, associated with gamma-ray burst (GRB) 170817A and kilonova AT2017gfo, has marked the start of a new era in astrophysics. GW170817 has confirmed that binary NS mergers are progenitors of at least some short GRBs. The peculiar properties of the GRB 170817A radio afterglow, characterized by a delayed onset related to the off-axis geometry, have also demonstrated how some nearby short GRBs may not be identified as such with standard short-timescale electromagnetic follow-up observations. Building upon this new information, we performed late-time radio observations of a sample of four short GRBs with unknown redshift and no previously detected afterglow in the Swift/BAT sample in order to identify nearby ($d_L \lesssim 200$ Mpc) off-axis GRB candidates via their potential late-time radio signatures. We find a previously uncatalogued radio source within the error region of GRB 130626 with a 3–6 GHz flux density consistent with an NS radio flare at a distance of ∼100 Mpc. An origin related to a persistent radio source unrelated to the GRB cannot be excluded nor confirmed given the high chance of false positives in error regions as large as those considered here, and the limited time baseline of our observations. Further radio (and X-ray) follow-up observations are needed to better understand the origin of this source.

Unified Astronomy Thesaurus concepts: Gravitational waves (678); Non-thermal radiation sources (1119); Radio continuum emission (1340); Gamma-ray bursters (1878)

1. Introduction

GW170817, the first binary neutron star (NS) merger detected by the LIGO and Virgo gravitational wave (GW) detectors, was accompanied by an electromagnetic (EM) counterpart observed in all bands of the EM spectrum (Abbott et al. 2017a, 2017b, 2017c and references therein). Located at ∼40 Mpc (e.g., Blanchard et al. 2017; Coulter et al. 2017), it was associated with the closest and most sub-energetic short γ-ray burst (GRB) we know of, GRB 170817A (Abbott et al. 2017a; Fong et al. 2017; Goldstein et al. 2017; Savchenko et al. 2017). GW170817 also provided the first direct evidence of a kilonova, a quasi-thermal UV-optical-IR transient powered by the radioactive decay of heavy elements (dubbed AT2019gfo; e.g., Arcavi et al. 2017; Chornock et al. 2017; Cowperthwaite et al. 2017; Coulter et al. 2017; Drout et al. 2017; Kasliwal et al. 2017; Nicholl et al. 2017; Soares-Santos et al. 2017; Valenti et al. 2017). The delayed afterglow of GRB 170817A, discovered in X-rays and radio ≈9 and ≈15 days after the merger, respectively, was unusual (Abbott et al. 2017c; Hallinan et al. 2017; Haggard et al. 2017; Troja et al. 2017). Indeed, we now know that GW170817 also represents the very first secure observation of an off-axis GRB (Alexander et al. 2017; Margutti et al. 2017; Corsi et al. 2018; Dobie et al. 2018; Margutti et al. 2018; Mooley et al. 2018a, 2018b, 2018c; Troja et al. 2018a; Ghirlanda et al. 2019; Hajela et al. 2019; Troja et al. 2019; Makhathini et al. 2020). The overall picture that has emerged via extended radio follow-up is that of a structured relativistic outflow with an energetic jet core of half opening angle $\theta_j \sim 5°$, accompanied by slower, less-energetic wings on larger angular scales (tens of degrees) from the jet axis (Granot et al. 2018; Lazzati et al. 2018; Mooley et al. 2018c). This structured jet is substantially different from the top-hat jet of uniform brightness typically assumed to model EM observations of cosmological GRBs (e.g., Berger 2014; van Eerten & MacFadyen 2012).

The new evidence for structured jets brought by GW170817/GRB 170817A, together with the surprising proximity of this event, have raised the question of whether the known sample of short GRBs could be hiding a nearby population of GW170817-like events. In fact, GW170817-like afterglows could have been missed by the typical localization strategy based on rapid X-ray and radio follow-up observations of GRBs. While a kilonova component similar to AT2017gfo would be well above the sensitivity of most ground-based telescopes up to distances of ≈200 Mpc, a kilonova fainter or redder than AT2017gfo (e.g., Metzger & Fernández 2014) could have been easily missed in past searches as well. On the other hand, the late-time radio flares predicted to arise by the interaction of the fastest kilonova ejecta with the circum-binary medium could still be detectable years after the GRB (e.g., Nakar & Piran 2011; Hotokezaka et al. 2013, 2016, 2018; Nakar 2020; Liu et al. 2020; Margalit & Piran 2020).

The above considerations have motivated a variety of studies aimed at hunting for nearby GRBs in the currently known sample of bursts, and at constraining their rate using potential late-time radio signatures (Gupte & Bartos 2018; Fong et al. 2016; Mandhai et al. 2018; Troja et al. 2018b; Yue et al. 2018; Bartos et al. 2019; Klose et al. 2019; von Kienlin et al. 2019;

Matsumoto & Piran 2020; Ricci et al. 2020; Schroeder et al. 2020). Other studies have also looked at the possibility of discovering late-time radio flares by kilonova ejecta using radio survey data alone (Law et al. 2018; Lee et al. 2020). Among the above studies, Mandhai et al. (2018) did not find any robust evidence for a population of local short GRBs and constrained their all-sky rate to $\lesssim 4$ yr^{-1} within 200 Mpc. Gupte & Bartos (2018) instead concluded that up to 10% of the total short GRB sample could be nearby. More recently, Dichiara et al. (2012) have cross-correlated short GRB positions with a catalog of nearby galaxies, and found four possible associations at 100 Mpc $\lesssim d_L \lesssim$ 200 Mpc. Ricci et al. (2020) followed-up these GRBs in the radio and set constraints on their potential radio flares based on radio non-detections.

Here, we focus on the sample of short GRBs presented in Bartos et al. (2019) as worth monitoring in the radio to uncover potential nearby events. The radio remnants of these nearby GRBs were estimated to still be potentially detectable by the Karl G. Jansky Very Large Array (VLA) if located within 200 Mpc (the advanced LIGO horizon distance for binary NS mergers when reaching design sensitivity; Abbott et al. 2018), and if their circum-merger medium is sufficiently dense. In Section 2 we briefly summarize the criteria we followed to select our GRB sample. We refer the reader to Bartos et al. (2019) for a more detailed description of the sample selection. In Section 3 we describe our radio follow-up observations and data reduction. In Section 4 we discuss our results, and in Section 5 we summarize and conclude.

2. GRB Sample Selection

To identify nearby GRB candidates in the Swift sample, we used the following criteria:

1. *Accurate gamma-ray localization*—Without a detected afterglow, a GRB is typically localized solely from its γ-ray emission and thus localization errors are larger than the arcsec localization radii of GRBs with early afterglow detections. In order to minimize the time required for deep radio follow-up, we thus restricted our selection to GRBs that had been observed with the Burst Alert Telescope (BAT) on-board the Neil Gehrels Swift Observatory (Gehrels et al. 2004). Bursts in this sample typically have 90% localization error radii and systematic uncertainties smaller than half the full width at half maximum of the VLA primary beam at 6 GHz (Lien et al. 2016). For our search, we queried the Swift-BAT catalog for GRBs detected between 2005 and 2018. This initial sample contained about 1200 GRBs.
2. *Short GRBs*—Next, we selected GRBs that were identified in the literature as short based on their duration (T_{90}) and spectral hardness (Kouveliotou et al. 1993). About 10% of the GRBs in the initial sample above passed this selection.
3. *Lack of an afterglow detection*—We further restrict our sample to only include those GRBs with no early afterglow detections, so as to specifically target potential off-axis events whose afterglow would become visible beyond the typical time frame of X-ray and optical follow-up observations. Only $\approx$2% of the GRBs in the initial sample met this requirement.
4. *Kilonova constraints*—We additionally exclude GRBs with sufficiently sensitive and timely optical follow-up observations that rule out a GW170817-like kilonova from the binary merger that produced the GRB, if the merger was within 200 Mpc. This left $\approx$1% of the GRBs in the initial sample. We note that while the kilonova optical luminosity constrains the ejecta mass and its characteristic velocity, it does not constrain a high-velocity ejecta tail which can contribute substantial radio emission (e.g., Kathirgamaraju et al. 2019). Quantitatively assessing the relative importance between optical and radio emission as related to different kilonova ejecta velocity distributions is beyond the scope of this paper. Here, we make the simplifying assumption that GW170817-like ejecta can be fully characterized via a two-component ejecta ($0.04\,M_\odot$ at speed $0.1c$ and $0.01\,M_\odot$ at speed $0.3c$; Bartos et al. 2019). Such a two-component ejecta can explain GW170817-like optical kilonovae, and may power visible radio flares that are the focus of this search (see Section 4).
5. *VLA observability and detectability*—Finally, to ensure observability of GRBs in our sample with the VLA, we excluded GRBs with decl. below -40° as these are too far South. Additionally, we excluded GRBs in the decl. range $[-5^\circ, 15^\circ]$, to avoid Radio Frequency Interference (RFI) associated with satellites in the Clarke Belt. Finally, we only considered events for which a realistic circum-merger density of $\lesssim 1$ cm^{-3}, and two observations in 2019 and 2020 with a reasonable VLA observing time, could potentially result in detections (assuming distances of 40 Mpc $\lesssim d_L \lesssim$ 200 Mpc; see Bartos et al. 2019, for more details). Only $\approx$0.7% of the GRBs in the initial sample met this final selection criteria.

None of the GRBs in our sample have cataloged galaxies within 200 Mpc that overlap with their localization (the catalog completeness on this distance scale is only 40% at present; Bartos et al. 2019). In what follows, we present VLA observations for four of the GRBs identified as described above. For these GRBs we were able to carry out two late-time VLA observations via our programs (VLA/19A-184 and VLA/20A-239; PI: Bartos).

3. VLA Follow-up Observations, Data Reduction, and Source Identification

Observations of the GRBs in our sample were carried out using the VLA in its C and B configurations. We observed all GRBs in two frequency bands centered at 3 GHz (*S*-band) and 6 GHz (*C*-band), for an overall frequency range of $\approx$2–8 GHz. A summary of our observations is reported in Table 1. Data calibration, imaging, source identification, and related measurements were carried out following a procedure similar to what is described in Artkop et al. (2019), which we briefly summarize in what follows. Results of our analysis are reported in Table 2.

The raw data were calibrated using the VLA automated calibration pipeline in `CASA` (McMullin et al. 2007). After the initial calibration, the data were further inspected and flagged as needed for residual RFI. Imaging was carried out using the `tclean` algorithm in interactive mode. All cleaned images were visually inspected to identify sources with signal-to-noise ratio (SNR) $\gtrsim$5. Source maximum flux densities and positions were calculated using `imstat` within a circular region of radius comparable to the full width at half maximum (FWHM)

Table 1
Sensitivity (rms) Reached in Our Observations of The GRBs in Our Sample

GRB Field Name	Freq. (GHz)	rms (μJy)	UT Date	ΔT[a] (days)
130626	6.2	7.3	08 Jul 2019	2203
"	5.2	15	29 Mar 2020	2468
"	2.9	12	24 Jul 2019	2219
141205	6.2	6.5	02 Apr 2019	1580
"	2.8	10	14 May 2019	1621
151228	6.2	8.6	20 Jun 2019	1270
"	6.2	10	21 May 2020	1606
"	2.9	15	17 Jul 2019	1297
170112	6.2	7.9	30 Mar 2019	808
"	6.3	20	27 Feb 2020	1142
"	2.8	20	16 May 2019	855

Note.
[a] Epoch (days since GRB trigger) of our observations.

of the nominal synthesized beam, centered around the location of the source as identified through visual inspection. Peak flux density errors were calculated as the quadrature sum of the image rms noise at the source location (which accounts for the telescope primary beam correction) and a systematic absolute flux calibration error. The last was assumed to be of 5% for all observations that used 3C286 as flux calibrator (Perley & Butler 2017), and of 10% for all observations that made use of 3C48 as flux calibrator (given the ongoing flaring behavior of this source).

Position errors were calculated by dividing the clean beam semimajor axis (as derived using the `imfit` task in `CASA`) by the SNR of the source. For sources with low SNR, position errors estimated using this procedure are more conservative than position errors returned by `imfit` (via elliptical Gaussian fits), while for sources with SNR $\gtrsim$10 the two methods are found to closely agree (to better than the estimated systematic position uncertainty, conservatively estimated to be of $\approx$0.1″; Helfand et al. 2015; Palliyaguru et al. 2016; Artkop et al. 2019). When the position error calculated as above is found to be smaller than the VLA systematic position uncertainty, we set the position error equal to this systematic uncertainty.

For all VLA sources identified in our images within the GRBs error regions, we searched for previously known radio sources co-located with them. The observed distribution of projected physical offsets of short GRBs from their host galaxies has a median of 5 kpc (Fong et al. 2010). For the short GRB population as a whole, $\gtrsim$25% have projected offsets of $\lesssim$10 kpc; and $\gtrsim$5% have projected offsets of $\gtrsim$20 kpc (Fong et al. 2010). Thus, searching for known sources located within 1′ of the position of our VLA sources (which at distances of 40–200 Mpc corresponds to a physical offsets of $\sim$10–50 kpc) leaves room to find not only coincident counterparts but also potential host galaxies. In light of the above, we queried the catalogs by the National VLA Sky Survey (NVSS; Condon et al. 1998), VLA FIRST (Becker et al. 1994), and the NASA/IPAC Extragalactic Database (NED; Helou et al. 1995), searching for the closest previously known radio source found within 1′ of each of our VLA sources. We also obtained quick-look images from the VLA Sky Survey (VLASS; Lacy et al. 2020) by searching for VLASS fields with phase centers within 1 deg of the VLA candidate position. Our results are summarized in Table 2.

3.1. GRB 130626

GRB 130626 triggered the Swift/BAT at 10:51:03 on 2013 June 26 UTC (De Pasquale et al. 2013). The refined analysis of the BAT data enabled the localization of the GRB to R.A.= 18:12:30.6 decl. = −09:31:29.9 (J2000), with a position uncertainty of 1.″8 (90% containment radius; Sakamoto et al. 2013).

We observed the field of GRB 130626 with the VLA in its BnA configuration starting at 03:19:34 on 2019 July 8 UT at 6 GHz, and at 05:35:12 on 2019 July 24 UT at 3 GHz. Our observations, including calibration, lasted a total of 1 hr in each band. The cleaned image central rms was $\approx$7.3μJy at 6.2 GHz and $\approx$12μJy at 2.9 GHz. One radio source was identified in both our 6 GHz and 3 GHz images within the 1.8′ position uncertainty of the BAT error circle for GRB 130626 (Sakamoto et al. 2013). No known radio source was found within 1′ of such source in NVSS, FIRST, or VLASS, while the closest source reported in NED is an infrared source (see Table 2).

To test for any variability of the radio counterpart candidate identified in our VLA images of the GRB 130626 field, we re-observed the field at 6 GHz starting at 13:44:31 on 2020 March 29 UT with the VLA in its C configuration. The clean image central rms was $\approx$15μJy at 5.2 GHz. This second VLA observation was affected by significant RFI which led us to flag all spectral windows with nominal central frequencies above 6.1 GHz. Based on our two observations of this field in this frequency band, we conclude that no significant flux density variation is found for the candidate radio counterpart of GRB 130626 over the timescales of our observations. A comparison of Epoch 1 data with imaging restricted to the same spectral channels that remained unflagged in Epoch 2 confirmed this result (see Table 2).

Using our first 6 GHz observation and the 3 GHz observation of the candidate radio source in the field of GRB 130626, we derive a spectral index of $\beta = -0.90 \pm 0.30$, where we adopt the notation $F_\nu \propto \nu^\beta$. Within the large errors, this spectral index is broadly compatible with optically thin synchrotron emission expected from radio flares of NS mergers (Nakar & Piran 2011), as well as with radio emission associated with star formation in galaxies ($-1.1 \lesssim \beta \lesssim -0.4$; Seymour et al. 2008). This spectral index is also not inconsistent, within the large errors, with $\beta > -0.6$ found for 90% of flat-spectrum AGN (e.g., Itoh et al. 2020, and references therein).

Finally, to test for the potential presence of extended radio emission and gain more information about the morphology of the radio candidate, we also calculate the compactness C defined as $C = F_{3\,\mathrm{GHz,int}}/F_{3\,\mathrm{GHz,peak}}$, i.e., the ratio of the integrated and peak fluxes as measured using the `imfit` task in `CASA`. We find $C = 1.038 \pm 0.089$, fully compatible with the range $0.9 < C < 1.5$ typically used in the classification of point-like radio sources at this same frequency (Mooley et al. 2013). This also agrees with the fact that an elliptical Gaussian fit of the source using `imfit` returns no evidence for extended morphology.

3.2. GRB 141205

GRB 141205 triggered the Swift/BAT at 14:51:45 on 2015 December 5 UT (Cummings et al. 2014). The refined analysis of the BAT data enabled the localization of the GRB to R.A.= 06:11:26.1, decl. = +37:52:32.2 (J2000), with a position

Table 2
Radio Sources Found within The BAT Error Region of GRBs in Our Sample

GRB Field Name	R.A. Decl.[a] (VLA) (hh:mm:ss deg:mm:ss)	Class[b]	Epoch[c] (MJD)	ΔT[d] (day)	ν[e] (GHz)	F_ν[f] (VLA) (mJy)	Offset[g] ($''$)	Pos.Err.[h] (VLA) ($''$)
130626	18:12:34.00 −09:30:02.6	IrS	58672.14	2203	5.2	0.103 ± 0.016	4.1	0.10
	18:12:34.00 −09:30:02.6	IrS	58688.27	2219	2.9	0.174 ± 0.015	4.1	0.23
	18:12:33.98 −09:30:02.5	IrS	58937.57	2468	5.2	0.137 ± 0.018	3.8	0.32
151228	14:16:03.76 −17:39:56.0	IrS	58654.05	1270	6.2	0.200 ± 0.013	0.12	0.10
	14:16:03.76 −17:39:55.8	IrS	58681.12	1297	2.9	0.445 ± 0.027	0.36	0.10
	14:16:03.73 −17:39:55.4	IrS	58990.08	1606	6.2	0.196 ± 0.014	0.84	0.43
170112	01:00:54.06 −17:12:43.6	IrS	58572.72	808	6.2	0.147 ± 0.020	13	0.17
	01:00:54.06 −17:12:43.5	IrS	58619.58	855	2.8	0.241 ± 0.030	13	0.43
	01:00:54.07 −17:12:43.7	IrS	58906.98	1142	6.3	0.151 ± 0.026	13	0.46

Notes.
[a] R.A. and decl. of the identified radio source(s) from our VLA images.
[b] Object class of the closest NED counterpart within 1′ radius of the VLA position. NED object type IrS stands for infrared source.
[c] Modified Julian Date (MJD) of our VLA observations.
[d] Epoch in days since the GRB trigger time.
[e] VLA nominal central frequency.
[f] VLA peak flux density.
[g] Offset between the source location as measured in our VLA images and that reported in NED.
[h] VLA position error.

uncertainty of 2.″0 (90% containment radius; Markwardt et al. 2014).

We observed the field of GRB 141205 with the VLA in its B configuration starting at 21:19:13 on 2019 April 2 UT at 6 GHz, and at 9:37:42 on 2019 May 14 UT at 3 GHz. Our observations, including calibration, lasted a total of 1 hr in each band. The clean image central rms was ≈6.5 μJy at 6.2 GHz and ≈10 μJy at 2.8 GHz. None of the sources identified in our VLA images are within the BAT 2.″0 error circle for this GRB.

3.3. GRB 151228A

GRB 151228 triggered the Swift/BAT at 03:05:12 on 2015 December 28 UT (Ukwatta et al. 2015). The refined analysis of the BAT data enabled the localization of the GRB to R. A. = 14:16:04.0 decl. = −17:39:52.7 (J2000), with a position uncertainty of 1.″8 (90% containment radius; Barthelmy et al. 2015)

We observed the field of GRB 151228 with the VLA in its B configuration starting at 01:10:08 on 2019 June 20 UT at 6 GHz, and in its BnA configuration at 02:46:55 on 2019 July 17 UT at 3 GHz. Our observations, including calibration, lasted a total of 1 hr in each band. The cleaned image central rms was ≈8.6μJy at 6.2 GHz and ≈15μJy at 2.9 GHz. One source identified in both our 6 GHz and 3 GHz images is found within the 1.″8 position uncertainty of the BAT error circle for GRB 151228 (Barthelmy et al. 2015). No known radio source was found within 1′ of such source in NVSS, FIRST, or VLASS, while the closest source reported in NED is an infrared source (see Table 2).

To test for any variability of this candidate radio counterpart, we re-observed the field of GRB 151228 at 6 GHz starting at 02:14:25 on 2020 May 21 UT with the VLA in its C configuration. The clean image central rms was ≈10μJy at 6.2 GHz. Based on our two observations of this field in this band, we conclude that no significant flux density variation is found for the identified VLA source over the timescales of our observations (see Table 2).

Using our first 6 GHz observation and the 3 GHz observation of the candidate radio source in the field of GRB 151228, we derive a spectral index of $\beta = -1.05 \pm 0.12$. This spectral index is compatible with optically thin synchrotron emission expected from radio flares of NS mergers (Nakar & Piran 2011), as well as with radio emission associated with star formation in galaxies ($-1.1 \lesssim \beta \lesssim -0.4$; Seymour et al. 2008). However, a flat spectrum ($\beta > -0.6$; Itoh et al. 2020) AGN is disfavored.

Finally, we find $C = 1.21 \pm 0.19$ for the compactness parameter, fully compatible with the range $0.9 < C < 1.5$ typically used in the classification of point-like sources at 3 GHz (Mooley et al. 2013). This also agrees with the fact that an elliptical Gaussian fit of the source using `imfit` returns no evidence for extended morphology.

3.4. GRB 170112

GRB 170112 triggered the Swift/BAT at 02:02:00 UTC on 2017 January 12 UT (Mingo et al. 2017). The refined analysis of the BAT data enabled the localization of the GRB to R.A.= 01:00:55.7, decl. = −17:13:57.9, (J2000), with a position uncertainty of 2.″5 (90% containment radius; Lien et al. 2017).

We observed the field of GRB 170112 with the VLA in its B configuration starting at 17:28:30 UTC on 2019 March 30, at 6 GHz, and at 13:57:23 on 2019 May 16 at 3 GHz. Our observations, including calibration, lasted a total of 1 hr in each band. The cleaned image central rms was ≈7.9μJy at 6.2 GHz and ≈20μJy at 2.8 GHz. One source identified in both our 6 GHz and 3 GHz images is found within the 2.5′ position uncertainty of the BAT error circle for GRB 170112 (Lien et al. 2017). No known radio source was found within 1′ of such a source in NVSS, FIRST, or VLASS, while the closest source reported in NED is an infrared source (see Table 2).

To test for any variability of the candidate VLA counterpart in the GRB 170112 field, we re-observed the field at 6 GHz starting at 23:37:08 on 2020 February 27 UT with the VLA in its C configuration. The clean image central rms was ≈20 μJy at 6.3 GHz (with the image being dynamic range limited due to the presence of two bright sources in the field). Based on our two observations of this field in this band, we conclude that no significant flux density variation is found for the identified

VLA source over the timescales of our observations (see Table 2).

Using our first 6 GHz observation and the 3 GHz observation of the candidate radio source in the field of GRB 151228, we derive a spectral index of $\beta = -0.62 \pm 0.18$. This spectral index is compatible with optically thin synchrotron emission expected from radio flares of NS mergers (Nakar & Piran 2011), with radio emission associated with star formation in galaxies ($-1.1 \lesssim \beta \lesssim -0.4$; Seymour et al. 2008), and with emission from a flat spectrum ($\beta > -0.6$; Itoh et al. 2020) AGN.

Finally, we find $C = 0.89 \pm 0.39$ for the compactness parameter, fully compatible with the range $0.9 < C < 1.5$ typically used in the classification of point-like sources at 3 GHz (Mooley et al. 2013). This also agrees with the fact that an elliptical Gaussian fit of the source using `imfit` returns no evidence for extended morphology.

4. Discussion

Among our sample of four GRBs, three (GRB 130626, GRB 151228, and GRB 170112; see Table 2) have a candidate VLA counterpart within their Swift/BAT localization region. None of these candidates showed significant time variability of the flux density at 5–6 GHz within the timescale of our observations (and our flux density measurement errors), and all of them have compactness C compatible with point sources at 3 GHz (Mooley et al. 2013). No radio source was found within $1'$ of our radio candidates in NVSS/FIRST/VLASS. We note that VLASS is conducted at 3 GHz, thus matching the *S*-band observations of GRBs in our sample. However, the rms values of the VLASS images containing the GRB fields is ≈0.17–0.18 mJy at 3 GHz, and thus it is not surprising that no significant radio excess was found around the position of our VLA candidate counterparts (whose 3 GHz flux is below the VLASS 3× rms sensitivity for these fields; see Table 2).

As discussed in Section 3, the spectral indices of the VLA candidate radio sources in Table 2 are compatible with both flares of binary NS mergers and star formation in galaxies. For two of our three GRBs, GRB 130626 and GRB 170112, the radio candidate has spectral index also compatible with a flat spectrum AGN, within the uncertainties.

In light of the above, in this Section we discuss the possible origin of the radio candidates identified in our GRB sample. We first quantify the chances of finding persistent and variable radio sources not related to GRB emission within error areas comparable to those of GRBs in our sample. Then, we discuss possible scenarios for the origin of these candidates in terms of AGN or star formation emission, as well binary NS merger radio flares.

4.1. Contaminating Persistent and Variable Radio Sources

Given the lack of significant temporal variability of the measured flux densities at 6 GHz (within the timescales and flux density measurement errors of our observations), we can estimate the number of persistent and unrelated radio sources one would expect in the Swift/BAT error area of GRBs in our sample. Using our spectral index measurement, we derive an upper-bound on the 1.4 GHz emission from these candidates counterparts of $F_{1.4\,\mathrm{GHz}} \lesssim 0.3 - 1$ mJy, assuming an optically thin spectrum. Mooley et al. (2013) have estimated the average number of persistent radio sources with 1.4 GHz flux densities $\gtrsim$0.1 mJy to be ≈910 deg^{-2}. The three GRBs for which we found a candidate VLA counterpart have 90% containment error radii of $1\farcm8$–$2\farcm5$, implying expected average numbers of *persistent* radio sources in their error regions of ≈2.6–5 per GRB. Thus, our results are consistent with potentially unassociated persistent radio sources in the GRB fields.

We note, however, that because we have collected only two epochs for each GRB in our sample, our assessment of lack of variability is restricted to poorly sampled timescales. Further follow-up could clarify whether the sources we have identified are truly persistent. As noted in Mooley et al. (2013), the variable/transient radio sky is a lot quieter than the persistent radio sky, with an average areal sky density of variable radio sources about 1% that of persistent radio sources. Thus, if the candidate radio sources identified here were found to be variable in future follow-up observations, the likelihood of a spurious association with the corresponding GRBs would be reduced, as ≈0.26–0.5 variable sources would be expected within the error circles of these GRBs. Consequently, the Poisson probability of finding one or more unrelated variable radio sources within the GRB error area would be 20%–40% for GRBs in our sample.

4.2. Testing an AGN or Star Formation Origin

Star-forming galaxies and AGNs are likely to be the two major populations of radio (cm) sources that could contribute false positives to a search for binary NS merger radio flares when dealing with relatively large localization areas (e.g., Condon 1992; Sadler et al. 1999; Smolčić et al. 2008; Baran et al. 2016; Palliyaguru et al. 2016). Below ≈200 μJy at 3 GHz, star-forming galaxies start to dominate in terms of fractional contribution to the total source sample (Baran et al. 2016), although low-luminosity AGNs may also be present (Mooley et al. 2013). At the mJy level, the transient/variable radio sky is dominated by AGNs (Sadler et al. 1999).

The compactness parameters and `imfit` size measurements for the VLA candidate radio sources found in our analysis do not provide clear evidence for extended emission, and suggest a point-like morphology within the VLA *S*-band resolution of $\approx 2\farcs7$–$3\farcs3$ (major axis FWHM of the synthesized beam in B configuration). We can compare this constraint with effective radii of short GRB host galaxies in the cosmological sample presented by Fong & Berger (2013). Those have effective radii in the range $0\farcs2$–$1\farcs2$, or ≈3.5 kpc in terms of median physical size. This median size would correspond to an angular radius of $\gtrsim 3\farcs9$ at distances $\lesssim$200 Mpc. Thus, if the radio candidates found in the GRBs' error regions were the host galaxies of the GRB themselves, our measurements would suggest distances $\gtrsim$200 Mpc to be more likely.

If all of the radio emission of the VLA candidates is associated with synchrotron radiation from relativistic electrons accelerated by supernovae in a normal galaxy, the implied star formation rate (SFR) can be estimated as (Murphy et al. 2011; Perley & Perley 2013):

$$\left(\frac{\mathrm{SFR}}{M_\odot\ \mathrm{yr}^{-1}}\right) = 6.35 \times 10^{-29}\left(\frac{L_{1.4\,\mathrm{GHz}}}{\mathrm{erg\ s^{-1}Hz^{-1}}}\right). \quad (1)$$

If we assume that the VLA candidates are associated with SFR in galaxies located at 200 Mpc, the implied luminosity densities would be in the range $L_{1.4\,\mathrm{GHz}} \lesssim (1.6\text{–}4.6) \times 10^{28}$ erg s^{-1} Hz^{-1}, and SFRs in the range SFR $\lesssim$ (1–2.8)$M_\odot$ yr^{-1}, compatible with normal galaxies. This is also compatible with

SFR rates of cosmological short GRB host galaxies, which are found to be in the range (0.2–6)$M_\odot$ yr^{-1}. The host galaxy of GW170817, NGC4993, had an uncommonly low SFR of 0.01 $M_\odot$ yr^{-1} (Fong et al. 2017).

On the other hand, if we assume the radio emission originated from a typical short GRB host galaxy at the median short GRB redshift of $z = 0.72$ (Berger 2014), the 1.4 GHz flux densities estimated above would imply luminosity densities of $L_{1.4\mathrm{GHz}} \lesssim (4 - 14) \times 10^{30}$ erg s^{-1} Hz^{-1} after accounting for redshift effects, (or, equivalently, radio power values of log ($L_{1.4\mathrm{GHz}}$[W/Hz]) $\lesssim 23.6 - 24.1$). Thus, under the cosmological GRB host galaxy hypothesis, and under the assumption of optically thin spectral indices down to 1.4 GHz, our measured flux densities would favor an AGN origin of the radio emission.

As a way to further differentiate between AGNs and normal galaxies, we can use WISE color information (Mateos et al. 2012) about our VLA candidates. Among our three VLA candidates, only the one associated with GRB 130626 has $W1$, $W2$, $W3$ colors and corresponding errors available in the WISE catalog. For this candidate we derive $W1 - W2 = -0.047 \pm 0.035$ and $W2 - W3 = 1.04 \pm 0.12$, which place this candidate out of the AGN wedge defined by $W2W3 > 2.517$ and $W1 - W2 > 0.315 \times (W2 - W3) - 0.222$ (Mateos et al. 2012), favoring an SFR origin over an AGN hypothesis.

4.3. Testing a Binary NS Merger Origin

We finally consider whether the VLA candidates identified in the error region of the GRBs in our sample could be consistent, in terms of flux densities in the 3–6 GHz range, with an NS merger radio flare origin.

To this end, we adopt an ejecta model similar to that observed for the case of GW170817. Specifically, we assume a two-component ejecta, with component masses 0.04 $M_\odot$ and 0.01 $M_\odot$, and speed of 0.1 c and 0.3 c, respectively (Bartos et al. 2019). We then simulate the expected radio light curves for a range of circum-merger densities ($n_{\mathrm{ISM}} = 10^{-4}$–10 cm^{-3}; Berger 2014) and distances (40–200 Mpc), and identify the density and distance parameters corresponding to the radio flare light curve that best matches the observed data.

We find that two of our three radio sources (those identified in the error regions of GRB 151228 and GRB 170112) cannot be adequately fit with this model. On the other hand, the observations corresponding to GRB 130626 can be fit with plausible model parameters. We show the data and the best-fit light curves for the two observed frequencies in Figure 1. This best-fit model corresponds to a circum-merger density of 7×10^{-2} cm^{-3} and a distance of 102 Mpc.

Assuming a spectral index similar to that observed for the radio-to-X-ray counterpart GW170817 ($\beta \approx -0.569$, see e.g., Makhathini et al. 2020), the ≈0.1 mJy flux density we measure at 5.2 GHz for the candidate counterpart of GRB 130626 implies a 0.3–10 keV un-absorbed flux of $\sim 5 \times 10^{-14}$ erg cm^{-1} s^{-1} at ≈2300 d since explosion. This is accessible to instruments such as Swift and Chandra, thus follow-up in the X-rays may also help constrain the origin of this candidate.

5. Summary and Conclusion

We have carried out VLA observations of a sample of four Swift short GRBs for which no afterglow was identified. Our observations aimed at discovering potential slowly-evolving radio counterparts from nearby binary NS mergers. For three out of the four GRBs in our sample we have found a corresponding VLA source not contained in previous radio catalogs.

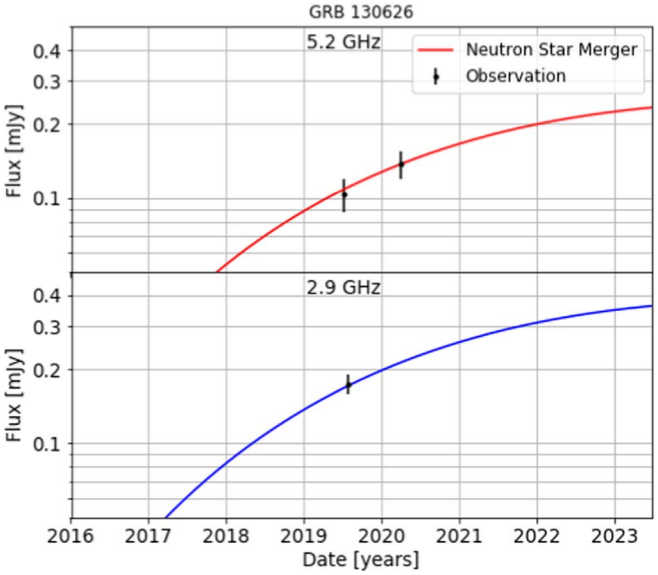

Figure 1. VLA follow-up observations in the direction of GRB 130626 at 5.2 GHz (top) and 2.9 GHz (bottom). We also show a comparison with an NS merger radio flare fit with NS merger time equal to the gamma-ray trigger time of GRB 130626, ejecta mass similar to that observed for GRB170817, circum-merger medium density of 7×10^{-2} cm^{-3}, and distance of 102 Mpc (solid lines).

Our VLA candidates did not show significant flux density variability within the limited time range (and flux density errors) of our observations. This is consistent with slowly-varying radio emission from an NS merger, or unrelated persistent radio sources. The fact that we found radio candidates within the GRB error areas is also consistent with expectations from the sky density of persistent radio sources.

The morphology of our radio candidates as estimated via the compactness parameter at 3 GHz disfavors an origin related to star formation in galaxies similar to that of short GRB hosts within 200 Mpc. On the other hand, the measured radio flux densities and spectral indices imply that an association with galaxies at a redshift equal to the median short GRB redshift would favor an AGN origin for the observed radio flux. For GRB 130626, available WISE observations do not support an AGN origin. However, an origin related to star formation in a galaxy at a distance larger than 200 Mpc (but smaller than the median short GRB redshift), with size similar to that of cosmological short GRB host galaxies, is plausible.

Finally, by fitting an NS merger radio flare model on our observations, we found that the radio source in the error region of GRB 130626 is consistent with the radio flare of an NS merger similar to GW170817, with circum-merger density of 7×10^{-2} cm^{-3} at a distance of 102 Mpc. Further radio (and X-ray) observations will be able to provide additional discrimination between the above scenarios for GRB 130626.

In conclusion, we note that under the optimistic assumptions that up to 10% of short GRBs in the known sample could be nearby (Gupte & Bartos 2018), the Poisson probability of detecting at least one of them in a sample of four GRBs is ≈33%, so searches like the ones here presented should continue

in a more systematic fashion. Targeting samples of $\gtrsim$23 GRBs would bring us to $\gtrsim$90% chances of detecting at least one event. Given the possible contamination from unrelated persistent radio sources, the follow-up campaign should be extended to several years so as to probe significant flux density variability. These types of radio follow-ups can be conducted on the VLA in filler-time mode, thus they are relatively inexpensive.

The authors are grateful to the anonymous Referee for providing constructive and extremely useful comments on the first version of this paper, and for suggesting to estimate the potential detectability of X-ray emission from the candidate radio counterpart of GRB 130626. The National Radio Astronomy Observatory is a facility of the National Science Foundation operated under cooperative agreement by Associated Universities, Inc. A.B., A.C., C.G., H.H., and P.R. acknowledge support from the National Science Foundation via the CAREER award #1455090 and award AST-1907975. J.M. acknowledges support from the Clark Scholars Program and Lubbock High School. I.B. acknowledges the support of the National Science Foundation under grant PHY-1911796 and the Alfred P. Sloan Foundation. Zs.M. and Sz.M. are grateful to National Science Foundation under grant PHY-1708028 and Columbia University in the City of New York for their generous support.

ORCID iDs

A. Corsi https://orcid.org/0000-0001-8104-3536
I. Bartos https://orcid.org/0000-0001-5607-3637

References

Abbott, B. P., Abbott, R., Abbott, T. D., et al. 2017a, ApJL, 848, L13
Abbott, B. P., Abbott, R., Abbott, T. D., et al. 2017b, PhRvL, 119, 161101
Abbott, B. P., Abbott, R., Abbott, T. D., et al. 2017c, ApJL, 848, L12
Abbott, B. P., Abbott, R., Abbott, T. D., et al. 2018, LRR, 21, 3
Alexander, K. D., Berger, E., Fong, W., et al. 2017, ApJL, 848, L21
Arcavi, I., Hosseinzadeh, G., Howell, D. A., et al. 2017, Natur, 551, 64
Artkop, K., Smith, R., Corsi, A., et al. 2019, ApJ, 884, 16
Baran, N., Smolcic, V., Delvecchio, I., et al. 2016, Active Galactic Nuclei: What's in a Name?, Vol. 15 (Munich: Zenodo)
Barthelmy, S., Cummings, J., Gehrels, N., et al. 2015, GCN, 18754
Bartos, I., Lee, K. H., Corsi, A., Márka, Z., & Márka, S. 2019, MNRAS, 485, 4150
Becker, R. H., White, R. L., & Helfand, D. J. 1994, in ASP Conf. Ser., 61, Astronomical Data Analysis Software and Systems III, ed. D. R. Crabtree, R. J. Hanisch, & J. Barnes (San Francisco, CA: ASP), 165
Berger, E. 2014, ARA&A, 52, 43
Blanchard, P. K., Berger, E., Fong, W., et al. 2017, ApJL, 848, L22
Chornock, R., Berger, E., Kasen, D., et al. 2017, ApJL, 848, L19
Condon, J. J. 1992, ARA&A, 30, 575
Condon, J. J., Cotton, W. D., Greisen, E. W., et al. 1998, AJ, 115, 1693
Corsi, A., Hallinan, G. W., Lazzati, D., et al. 2018, ApJL, 861, L10
Coulter, D. A., Foley, R. J., Kilpatrick, C. D., et al. 2017, Sci, 358, 1556
Cowperthwaite, P. S., Berger, E., Villar, V. A., et al. 2017, ApJL, 848, L17
Cummings, J. 2014, GCN, 17137
De Pasquale, M., Barthelmy, S., Burrows, D., et al. 2013, GCN, 14931
Dichiara, S., Troja, E., O'Connor, B., et al. 2012, MNRAS, 492, 5011
Dobie, D., Kaplan, D. L., Murphy, T., et al. 2018, ApJL, 858, L15
Drout, M. R., Piro, A. L., Shappee, B. J., et al. 2017, Sci, 358, 1570
Fong, W., & Berger, E. 2013, ApJ, 776, 18
Fong, W., Berger, E., Blanchard, P. K., et al. 2017, ApJL, 848, L23
Fong, W., Berger, E., & Fox, D. B. 2010, ApJ, 708, 9
Fong, W., Metzger, B. D., Berger, E., & Özel, F. 2016, ApJ, 831, 141
Gehrels, N., Chincarini, G., Giommi, P., et al. 2004, ApJ, 611, 1005
Ghirlanda, G., Salafia, O. S., Paragi, Z., et al. 2019, Sci, 363, 968
Goldstein, A., Veres, P., Burns, E., et al. 2017, ApJL, 848, L14
Granot, J., Gill, R., Guetta, D., & De Colle, F. 2018, MNRAS, 481, 1597
Gupte, N., & Bartos, I. 2018, arXiv e-prints, arXiv:1808.06238
Haggard, D., Nynka, M., Ruan, J. J., et al. 2017, ApJL, 848, L25
Hajela, A., Margutti, R., Alexander, K. D., et al. 2019, ApJL, 886, L17
Hallinan, G., Corsi, A., Mooley, K. P., et al. 2017, Sci, 358, 1579
Helfand, D. J., White, R. L., & Becker, R. H. 2015, ApJ, 801, 26
Helou, G., Madore, B. F., Schmitz, M., et al. 1995, in The NASA/IPAC Extragalactic Database, ed. D. Egret & M. A. Albrecht (Berlin: Springer), 95
Hotokezaka, K., Kiuchi, K., Kyutoku, K., et al. 2013, PhRvD, 87, 024001
Hotokezaka, K., Kiuchi, K., Shibata, M., Nakar, E., & Piran, T. 2018, ApJ, 867, 95
Hotokezaka, K., Nissanke, S., Hallinan, G., et al. 2016, ApJ, 831, 190
Itoh, R., Utsumi, Y., Inoue, Y., et al. 2020, ApJ, 901, 3
Kasliwal, M. M., Nakar, E., Singer, L. P., et al. 2017, Sci, 358, 1559
Kathirgamaraju, A., Giannios, D., & Beniamini, P. 2019, MNRAS, 487, 3914
Klose, S., Nicuesa Guelbenzu, A. M., Michałowski, M. J., et al. 2019, ApJ, 887, 206
Kouveliotou, C., Meegan, C. A., Fishman, G. J., et al. 1993, ApJL, 413, L101
Lacy, M., Baum, S. A., Chandler, C. J., et al. 2020, PASP, 132, 035001
Law, C. J., Gaensler, B. M., Metzger, B. D., Ofek, E. O., & Sironi, L. 2018, ApJL, 866, L22
Lazzati, D., Perna, R., Morsony, B. J., et al. 2018, PhRvL, 120, 241103
Lee, K. H., Bartos, I., Privon, G. C., Rose, J. C., & Torrey, P. 2020, ApJL, 902, L23
Lien, A., Barthelmy, S., Cummings, J., et al. 2017, GCN, 20436
Lien, A., Sakamoto, T., Barthelmy, S. D., et al. 2016, ApJ, 829, 7
Liu, L.-D., Gao, H., & Zhang, B. 2020, ApJ, 890, 102
Makhathini, S., Mooley, K. P., Brightman, M., et al. 2020, arXiv e-prints, arXiv:2006.02382
Mandhai, S., Tanvir, N., Lamb, G., Levan, A., & Tsang, D. 2018, Galax, 6, 130
Margalit, B., & Piran, T. 2020, MNRAS, 495, 4981
Margutti, R., Alexander, K. D., Xie, X., et al. 2018, ApJL, 856, L18
Margutti, R., Berger, E., Fong, W., et al. 2017, ApJL, 848, L20
Markwardt, C., Barthelmy, S., Baumgartner, W., et al. 2014, GCN, 17140
Mateos, S., Alonso-Herrero, A., Carrera, F. J., et al. 2012, MNRAS, 426, 3271
Matsumoto, T., & Piran, T. 2020, MNRAS, 492, 4283
McMullin, J. P., Waters, B., Schiebel, D., Young, W., & Golap, K. 2007, in ASP Conf. Ser. 376, Astronomical Data Analysis Software and Systems XVI, ed. R. A. Shaw, F. Hill, & D. J. Bell, 127
Metzger, B. D., & Fernández, R. 2014, MNRAS, 441, 3444
Mingo, B., Burrows, D., Gronwall, C., et al. 2017, GCN, 20436
Mooley, K. P., Deller, A. T., Gottlieb, O., et al. 2018c, Natur, 561, 355
Mooley, K. P., Frail, D. A., Dobie, D., et al. 2018b, ApJL, 868, L11
Mooley, K. P., Frail, D. A., Ofek, E. O., et al. 2013, ApJ, 768, 165
Mooley, K. P., Nakar, E., Hotokezaka, K., et al. 2018a, Natur, 554, 207
Murphy, E. J., Condon, J. J., Schinnerer, E., et al. 2011, ApJ, 737, 67
Nakar, E. 2020, PhR, 886, 1
Nakar, E., & Piran, T. 2011, Natur, 478, 82
Nicholl, M., Berger, E., Kasen, D., et al. 2017, ApJL, 848, L18
Palliyaguru, N. T., Corsi, A., Kasliwal, M. M., et al. 2016, ApJL, 829, L28
Perley, D. A., & Perley, R. A. 2013, ApJ, 778, 172
Perley, R. A., & Butler, B. J. 2017, ApJS, 230, 7
Ricci, R., Troja, E., Bruni, G., et al. 2020, MNRAS, 500, 1708
Sadler, E. M., McIntyre, V. J., Jackson, C. A., & Cannon, R. D. 1999, PASA, 16, 247
Sakamoto, T., Barthelmy, S., Baumgartner, W., et al. 2013, GCN, 14942
Savchenko, V., Ferrigno, C., Kuulkers, E., et al. 2017, ApJL, 848, L15
Schroeder, G., Margalit, B., Fong, W.-F., et al. 2020, ApJ, 902, 82
Seymour, N., Dwelly, T., Moss, D., et al. 2008, MNRAS, 386, 1695
Smolčić, V., Schinnerer, E., Scodeggio, M., et al. 2008, ApJS, 177, 14
Soares-Santos, M., Holz, D. E., Annis, J., et al. 2017, ApJL, 848, L16
Troja, E., Piro, L., Ryan, G., et al. 2018a, MNRAS, 478, L18
Troja, E., Piro, L., van Eerten, H., et al. 2017, Natur, 551, 71
Troja, E., Ryan, G., Piro, L., et al. 2018b, NatCo, 9, 4089
Troja, E., van Eerten, H., Ryan, G., et al. 2019, MNRAS, 489, 1919
Ukwatta, T., Barthelmy, S., Cummings, J., et al. 2015, GCN, 18731
Valenti, S., Sand, D. J., Yang, S., et al. 2017, ApJL, 848, L24
van Eerten, H. J., & MacFadyen, A. I. 2012, ApJ, 751, 155
von Kienlin, A., Veres, P., Roberts, O. J., et al. 2019, ApJ, 876, 89
Yue, C., Hu, Q., Zhang, F.-W., et al. 2018, ApJL, 853, L10